

Article published in:

*Cerebral Cortex*, 2014 Sep;24(9):2436-48. doi: [10.1093/cercor/bht098](https://doi.org/10.1093/cercor/bht098) Epub 2013 Apr 18.

## Connectivity architecture and subdivision of the human inferior parietal cortex revealed by diffusion MRI

Michael Ruschel<sup>1</sup>, Thomas R. Knösche<sup>1</sup>, Angela D. Friederici<sup>2</sup>, Robert Turner<sup>3</sup>,  
Stefan Geyer<sup>3,\*</sup>, Alfred Anwander<sup>1,2,\*,#</sup>

<sup>1</sup> Research Group “Cortical Networks and Cognitive Functions”,

<sup>2</sup> Department of Neuropsychology,

<sup>3</sup> Department of Neurophysics, Max Planck Institute for Human Cognitive and Brain Sciences, Leipzig, Germany

\*S.G. and A.A. share senior authorship.

### #Corresponding Author

Alfred Anwander Ph.D.  
Max Planck Institute for Human Cognitive and Brain Sciences,  
Department of Neuropsychology,  
Stephanstrasse 1a,  
04103 Leipzig  
Germany  
<http://www.cbs.mpg.de/~anwander>

## **Abstract**

The human inferior parietal cortex convexity (IPCC) is an important association area, which integrates auditory, visual and somatosensory information. However, the structural organization of the IPCC is a controversial issue. For example, cytoarchitectonic parcellations reported in the literature range from two to seven areas. Moreover, anatomical descriptions of the human IPCC are often based on experiments in the macaque monkey. In this study we used diffusion-weighted magnetic resonance imaging (dMRI) combined with probabilistic tractography to quantify the connectivity of the human IPCC, and used this information to parcellate this cortex area. This provides a new structural map of the human IPCC, comprising three sub-areas (IPC<sub>a</sub>, IPC<sub>m</sub>, IPC<sub>p</sub>) of comparable size, in a rostro-caudal arrangement in the left and right hemisphere. Each sub-area is characterized by a connectivity fingerprint and the parcellation is similar to the subdivision reported for the macaque IPCC (rostro-caudal areas areas PF, PFG, and PG). However, the present study also reliably demonstrates new structural features in the connectivity pattern of the human IPCC, which are not known to exist in the macaque. This study quantifies inter-subject variability by providing a population representation of the sub-area arrangement, and demonstrates substantial lateralization of the connectivity patterns of IPCC.

**Keywords:** connectivity based parcellation, diffusion MRI, DTI, human parietal lobe, inferior parietal cortical convexity, probabilistic tractography

## Introduction

The human inferior parietal cortex convexity (IPCC) is an important association area, which integrates auditory, visual and somatosensory information. This region plays a prominent role in visuospatial attention, especially in the right hemisphere, and in particular in the stimulus-driven ventral fronto-parietal attention network. In contrast, the superior posterior parietal lobe is (bilaterally) engaged in the more endogenously driven dorsal attention network (Corbetta and Shulman 2002). A second important area of involvement for the IPCC is in episodic memory retrieval. Paralleling the dichotomy of their involvement in the attention networks, the superior parietal cortex is more associated with endogenous or voluntary processes, while the IPCC supports processes like recollection, driven by external events (Cabeza et al. 2008; Vilberg and Rugg 2008). Moreover, in the left hemisphere, the IPCC is an important constituent of the cortical language network (Sakai et al. 2001; Binder et al. 2009; Graves et al. 2010; Hartwigsen et al. 2010; Price 2010).

There is evidence that the IPCC can be further subdivided into functional sub-areas. For example, familiarity based episodic memory effects are primarily found in the rostral part of IPCC (approximately the supramarginal gyrus; Cabeza et al. 2008; Vilberg and Rugg 2008). This same rostral area is related to covert articulation and phonological decision/mapping within the language network, while the caudal part of IPCC (approximately the angular gyrus) is involved in semantic retrieval (Vigneau et al. 2006; Binder et al. 2009; Graves et al. 2010; Price 2010).

Hence, the IPCC accommodates a rich variety of cognitive functionality, which maps onto distinct functionally specialized sub-areas. This is likely to be paralleled by a similar structural organization of anatomically distinct sub-areas. However, this subdivision remains a controversial issue. Brodmann (1909), in his "classical" cytoarchitectonic map, subdivided the IPCC into two regions: rostral area 40 (on the supramarginal gyrus) and caudal area 39 (on the angular gyrus). Subsequent investigators, using cytoarchitecture (von Economo and Koskinas 1925; Gerhardt 1940; Sarkissov et al. 1955) or myeloarchitecture (Vogt 1911; Batsch 1956), parcellated the IPCC into a higher number of regions, each characterized by a specific regional architectonic layout (termed "sub-areas" or "subregions"). A recent study (Caspers et al. 2006), using state-of-the-art observer-independent cytoarchitectonic mapping (Schleicher et al. 1999), found seven areas in the IPCC: five in its rostral part (broadly equivalent to Brodmann area 40) and two in its caudal part (broadly equivalent to Brodmann area 39). Subsequently, Caspers and colleagues (2013) used receptor mapping and showed that these seven areas could be clustered into three larger rostro-caudally arranged regions.

In the macaque monkey the situation is more straightforward. The "classical" cyto- and myeloarchitectonic literature identified one (Brodmann 1909) or two (Vogt and Vogt 1919; von Bonin and Bailey 1947) regions. Multimodal studies employing architectonic mapping (Pandya and Seltzer 1982; Gregoriou et al. 2006), *in vitro* autoradiography of the distribution of neurotransmitter binding sites (Geyer et al. 2005), tract tracing (Pandya and Seltzer 1982; Rozzi et al. 2006), and electrophysiology (Rozzi et al. 2008) converge on a parcellation into four regions: PF, PFG, PG, and Opt – aligned in a rostro-caudal arrangement along the longitudinal axis of the IPCC. The nomenclature of the areas were proposed by Pandya and Seltzer (1982) based on the initial naming convention by Bonin and Bailey (1947). The four areas markedly differ in their architectonic organization (cytoarchitecture, myeloarchitecture, regional distribution of neurotransmitter binding sites and immunoreactivity; Geyer et al. 2005; Gregoriou et al. 2006), frontal, parietal and temporal cortical connections (Rozzi et al. 2006), and in the somatosensory, visual, and motor responses of their neurons (Rozzi et al. 2008). However, despite this extensive characterization, their possible homologues in humans are still unclear.

In humans, a different perspective may shed new light on this old problem: not only cyto- or myeloarchitecture, but also connectivity patterns can structurally (and therefore, also functionally) characterize cortical areas. Diffusion-weighted magnetic resonance imaging (dMRI), combined with probabilistic tractography, elegantly measures such connectivity patterns non-invasively in living participants (Johansen-Berg et al. 2004; Anwander et al. 2007). This technique can be used to compute connectivity fingerprints that characterize the connectivity of a brain area under investigation with a collection of preselected target areas. For example, Behrens and colleagues (2003) parcellated the human thalamus, according to its connectivity to a number of macroanatomically defined cortical regions. More recently, Rushworth and colleagues (2006) used probabilistic tractography to characterize the connectivity profile of 6 predefined target regions in the lateral parietal cortex with 3 predefined regions elsewhere in the brain (superior colliculus, parahippocampal gyrus, ventral premotor cortex), which are known to project differentially to three distinct regions in macaque parietal cortex. They provide a detailed comparison of the connection pathways between these areas to corresponding pathways in the macaque brain.

A different, less hypothesis driven, approach exploits the fact that probabilistic tractography is able to estimate the connectivity profile of each point in a region of interest (ROI; here the IPCC) to the rest of the brain. With an automatic clustering algorithm, cortical regions can then be identified, which feature internally coherent but mutually distinct connectivity (Anwander et al. 2007). This approach has been successfully applied to parcellate the medial premotor cortex into supplementary and pre-supplementary motor areas (Johansen-Berg et al. 2004), the lateral premotor

cortex into its dorsal and ventral subregions (Tomassini et al. 2007; Schubotz et al. 2010), Broca's area into Brodmann areas (BA) 44 and 45 (Anwander et al. 2007; Klein et al. 2007), and the cingulate cortex into anterior, midcingulate, and posterior subregions (Beckmann et al. 2009). Very recently, Mars and colleagues (2011) investigated the right parietal cortex, including the IPCC, using mixed anatomical criteria: areas had to be both compact and similarly connected as measured with diffusion MRI. A region of interest that included the anterior parts of the occipital lobe and the parietal operculum was subdivided into five areas, arranged along the rostral-caudal axis. Additionally, they investigated functional connectivity from parietal cortex to some frontal and medio-temporal target areas using fMRI resting state activity in both macaque monkeys and humans.

If human and macaque IPCC are indeed homologous brain regions, their long-range connectivity<sup>1</sup> patterns should be similar. This has been demonstrated recently by Caspers and colleagues (2011), who compared tract tracing results from macaques with probabilistic tractograms of cytoarchitecturally predefined areas in humans.

Here, in contrast to the work of Caspers and colleagues (2011), we used dMRI probabilistic tractography, not only to characterize the connectivity profiles of IPCC sub-areas, but also to define these sub-areas in the first place. In extension to the work of Mars and colleagues (2011), we aimed at studying inter-hemispherical differences and similarities in IPCC structural organization in the light of the known strong functional lateralization (see above), at directly comparing anatomical parcellation and connectivity of IPCC to the connectional architecture of macaque IPCC (based on "classical" tract tracing), and at assessing the inter-individual variance of the parcellation results and the associated connectivity patterns. The results will help to resolve the question of whether or not there is a fine-grained homology between human and macaque IPCC.

## **Materials and Methods**

### ***Participants***

Twenty right-handed volunteers (10 males, 10 females, age  $25.5 \pm 3.5$  years) participated in the study. All participants gave written informed consent before being included in the experiment. The participants had no history of neurologic, psychiatric, or other major medical disorders and did not take any medication at the time of data acquisition. The experimental setup was approved by the local ethics committee of the University of Leipzig, Germany. Data were handled anonymously.

---

<sup>1</sup> The term „long-range connectivity“ here refers to fiber connections that run through the white matter, as opposed to „short-range“ intracortical connections.

### ***Data acquisition and preprocessing***

We acquired diffusion-weighted and high-resolution 3-dimensional (3D) T1-weighted images on a Siemens 3T Trio scanner with an 8-channel array head coil and maximum gradient strength of 40 mT/m. For the diffusion-weighted MR images (dMRIs) we employed a spin-echo echo planar imaging (EPI) sequence (TR = 12 s, TE = 100 ms, 72 axial slices, resolution  $1.7 \times 1.7 \times 1.7$  mm, no cardiac gating, 60 diffusion directions evenly distributed over the hemisphere, b-value = 1000  $\text{s}/\text{mm}^2$ ). In addition, we acquired seven data sets with no diffusion weighting, first at the beginning and then after each block of ten diffusion-weighted images, to serve as anatomical reference for motion correction. To increase signal-to-noise ratio (SNR), we repeated the measurement three times, resulting in a total scan time of approximately 45 min. For the high-resolution T1-weighted images we employed a 3D gradient echo (MPRAGE) sequence (TR = 1300 ms, TI = 650 ms, TE = 3.97 ms, flip angle  $10^\circ$ , 176 sagittal slices, resolution  $1.0 \times 1.0 \times 1.0$  mm, 2 repetitions, total scan time 12 min).

We reoriented the T1-weighted images to the sagittal plane through the anterior and posterior commissures and used the images without diffusion weighting to estimate motion correction parameters using rigid-body transformations (Jenkinson et al. 2002), implemented in FSL<sup>2</sup> (FMRIB Software Library, University of Oxford). We combined the motion correction for the dMRI data with the global registration to the T1 anatomy, corrected the gradient directions of each volume with the rotation parameters, interpolated the registered images to an isotropic voxel resolution of 1 mm, and averaged each subject's three acquisitions. Finally, we computed the diffusion tensor, the three eigenvectors, and the fractional anisotropy (FA) value for each voxel (Basser et al. 1994). The FA image was used to create a mask for the tractography including brain white matter and neighboring gray matter (threshold:  $\text{FA} > 0.08$ ). By rigid mapping of the diffusion images and the gradient directions to the standardized anatomical space, we were able to perform tractography in a common anatomical space. The rigid registration of all dMRIs to the slightly rotated T1 space introduces the same amount of smoothing (caused by the interpolation) to all dMRIs. This reduces a potential directional bias which might be caused by a varying amount of interpolation for the different dMRIs in the motion correction procedure. Additionally, the registration to the T1 space circumvented additional alignments steps after the preprocessing without altering the tractography results compared to a tracking procedure in the native diffusion space. This was confirmed by computing the cross-correlation between the tractograms computed in the two different spaces, quantified by a high correlation value (mean correlation in one ROI = 0.85, SD: 0.02).

---

<sup>2</sup> <http://www.fmrib.ox.ac.uk/fsl>

### ***Definition of the region of interest***

Initially, the ROI for tractography and parcellation were manually defined simultaneously on the pial and inflated white matter surfaces (Fischl et al. 1999) as generated by FreeSurfer<sup>3</sup> (Martinos Center for Biomedical Imaging, Boston). Since we focused our analysis on the convexity of the inferior parietal cortex, we excluded areas lying in the depth of the intraparietal sulcus (IPS), postcentral sulcus, and parietal operculum. Hence, we chose macroanatomical landmarks on or close to the exposed cortical surface as borders of the ROI: the lateral lip of the intraparietal sulcus (1 in Fig. 1A), the caudal lip of the postcentral sulcus (2 in Fig. 1A), the dorsal lip of the lateral fissure (3 in Fig. 1A), and the caudal shoulder of the angular gyrus (4 in Fig. 1A). The neighboring two cytoarchitectonically and functional different areas hIP1 and hIP2 in the IPS (Choi et al. 2006) which extend up to the shoulder of the sulcus were assured not to be part of the ROI. For the correct identification of the sulci, we used the “Atlas of the Cerebral Sulci” (Ono et al. 1990) to analyze the sulcal variability.

As a second step, we transformed the defined surface patches into voxel space and interactively labeled in coronal slices (using Anatomist<sup>4</sup>, Service Hospitalier Frédéric Joliot, CEA, Orsay, France) all voxels at the grey-white matter interface within the ROI (1 in Fig. 1B), as defined from the co-registered dMRIs (FA threshold 0.15). These voxels were used as seed points for subsequent diffusion tractography (2 in Fig. 1B). Voxels in the fundus of the bordering sulci were excluded to prevent connections with deep white matter structures in the parietal lobe like the long segment of the arcuate fascicle (Catani et al. 2005).

---

<sup>3</sup> <http://surfer.nmr.mgh.harvard.edu>

<sup>4</sup> <http://anatomist.info>

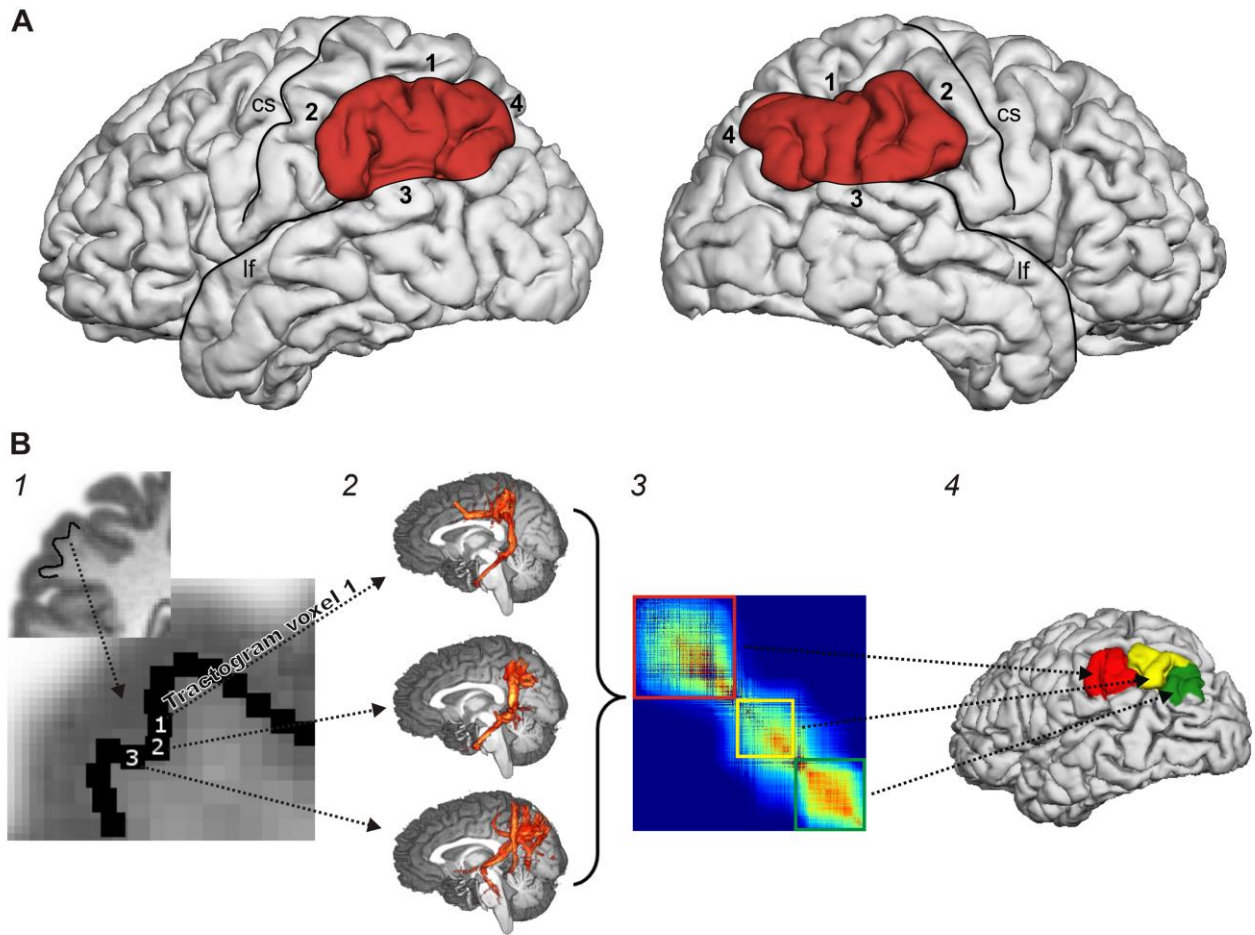


Fig. 1. A: Inferior parietal cortex ROI on a representative subject. (1) intraparietal sulcus / lateral lip; (2) postcentral sulcus / caudal lip; (3) lateral fissure / dorsal lip; (4) angular gyrus / caudal shoulder; cs = central sulcus; lf = lateral fissure.

B: General methodology of connectivity-based cortex parcellation. (1) Seed voxels for probabilistic tractography are placed in white matter at the grey-white matter interface of the IPCC. (2) For each of these voxels, a probabilistic tractogram is computed. (3) The matrix containing the correlations between all these tractograms is divided into clusters of voxels with similar correlation to the tractograms of other voxels. (4) Each of these clusters corresponds to a certain area on the cortical surface.

### ***Tractography and connectivity-based parcellation***

We used the probabilistic tractography method and the connectivity based parcellation scheme similar to the one proposed by Anwander and colleagues (2007). The underlying concept of connectivity-based parcellation is that cortical areas with similar anatomical connectivity are combined into a region, which is segregated from neighboring regions with different connectivity. The connectivity pattern of a cortical voxel is approximated by the tractogram associated with its immediately underlying white matter voxel. Fig. 1B illustrates the general principle of the

parcellation technique. For each seed voxel within the ROI (1 in Fig. 1B), we computed a probabilistic tractogram (2 in Fig. 1B) and arranged the correlation values between any two of these tractograms in a connectivity correlation matrix. In contrast to Anwander and colleagues (2007), who used a k-means clustering approach in order to define groups of voxels with similar connectivity (3 in Fig. 1B), we applied a cluster algorithm based on a Gaussian Mixture Model (as implemented in MatLab™) to the columns of the connectivity correlation matrix. This technique is better suited to cope with clusters showing differences in intra-cluster homogeneity (Gorbach et al. 2011).

A challenge for any clustering method is the trade-off between model consistency (how well does the clustering describe the structure of the data) and model complexity (preference of a simple model that describes the relevant features and ignores noise). Here, the clusters had to be defined *a priori*. We tested different numbers of clusters ( $2 \leq n \leq 7$ ), but accepted only those solutions that were consistent across hemispheres and participants, i.e., the principal arrangement of cortical areas (e.g., from inferior to superior or from anterior to posterior) associated with the clusters had to be the same. As a second requirement, each area had to represent a single topologically compact region of the cortex. Additionally, we characterized each area by its tractographic signature (i.e. its average tractogram). As a final step, we mapped the resulting clusters back onto the cortical surface of each individual brain (4 in Fig. 1B). The fact that this clustering approach yields neuroanatomically meaningful results has been substantiated in recent publications (Johansen-Berg et al. 2005; Anwander et al. 2007; Beckmann et al. 2009; Schubotz et al. 2010).

For interpretation of the parcellation results we first assessed the positions (computed as center-of-mass, in Talairach coordinates) and sizes (by voxel counting) of all IPCC sub-areas in all participants and hemispheres. We computed mean and standard deviation of these values for all participants.

In order to assess each area's topographical variability, we computed for each cluster a population overlap map. Therefore, we dilated the clusters (voxels at the grey-white matter interface) by 3 mm orthogonally to the surface and normalized all individual brains and clusters to the Montreal Neurological Institute (MNI) single subject brain (known as "colin27"), superimposed them in 3D space, and computed the population maps (see Fig. 5). This map shows, for each cluster and each voxel in MNI space, how many brains ( $0 \leq n \leq 20$ ) have a representation of this cluster in the particular voxel.

### *Connectivity analysis*

We qualitatively assessed the global connectivity profile of each IPCC sub-area by mapping the values of its tractographic signature. The seed regions for the tractography were derived from the population map with a minimum overlap of 5 participants. Seed voxels within overlapping areas were assigned to the sub-area with the maximum probability value. For tractography, the seed regions were morphed to the single subject brains. The connectivity was computed using a total of 100,000 random walks (cf. Anwander et al. 2007) per seed region. The single subject connectivity patterns were normalized to the MNI brain, and averaged over all participants. The average connectivity values in the grey-white matter interface were visualized on an inflated cortex representation of the MNI brain (Fig. 6). In order to quantitatively compare the connectivity patterns between the sub-areas, and thereby establish significant differences between these areas in terms of long-range connectivity, we analyzed each area's connectivity strength with specific target regions for all participants separately. For this purpose, we interactively defined 10 gyrus-based target ROIs (on the average brain over 20 participants; see Fig. 2).

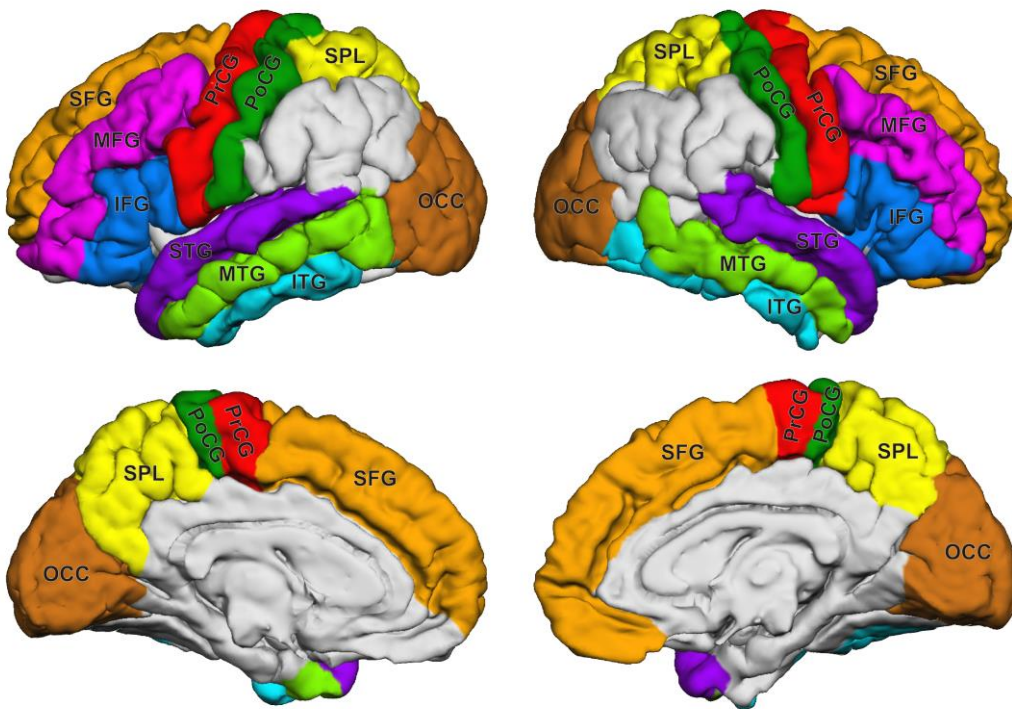


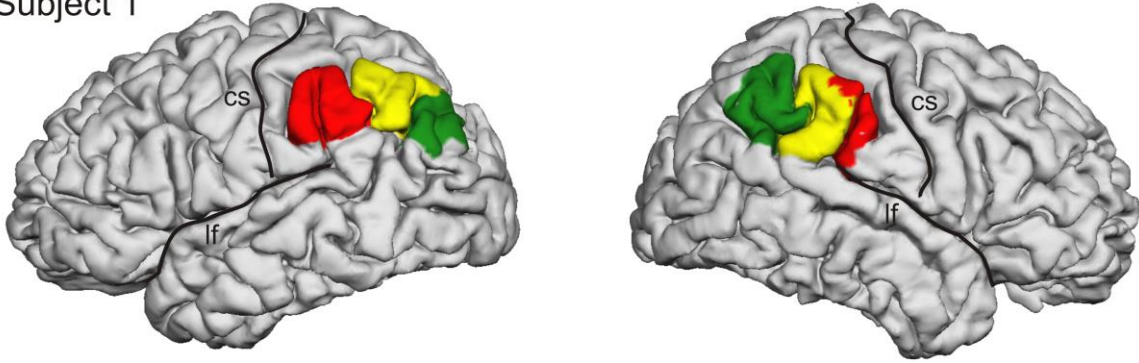
Fig. 2. Gyrus-based target ROIs superimposed on the mean brain of all 20 participants in MNI space. SFG = superior frontal gyrus; MFG = middle frontal gyrus; IFG = inferior frontal gyrus; PrCG = precentral gyrus; PoCG = postcentral gyrus; SPL = superior parietal lobule; STG = superior temporal gyrus; MTG = middle temporal gyrus; ITG = inferior temporal gyrus; OCC = occipital lobe.

These target ROIs were defined by macroanatomical landmarks (sulci) on the inflated brain surface by manual refinement of the automatic gyrus labeling computed by FreeSurfer (Martinos Center for Biomedical Imaging, Boston). The labeled cortical regions were mapped to the brain volume, and warped by non-linear registration of the mean brain to the individual T1-anatomy of the 20 participants. The correct warping of the target regions were manually validated in every individual subject. Analog to the seed ROI definition, we labeled all voxels at the grey-white matter interface within each region as target voxels. On a single participant basis (and separately for each hemisphere), we computed how many of the random walks starting in each IPCC sub-area reached each target. For statistical analysis of these connectivity values, which cannot be assumed to follow a normal distribution, we used the non-parametric Friedman repeated measures analysis of variance model (factor 1: IPCC area, factor 2: target; each hemisphere treated separately) and a Wilcoxon signed rank test for *post hoc* pairwise comparisons between the levels of factor 1 (i.e., IPCC areas). All  $p$  values were Bonferroni corrected for multiple comparisons. For testing connectivity differences between the hemispheres, the same procedure was used.

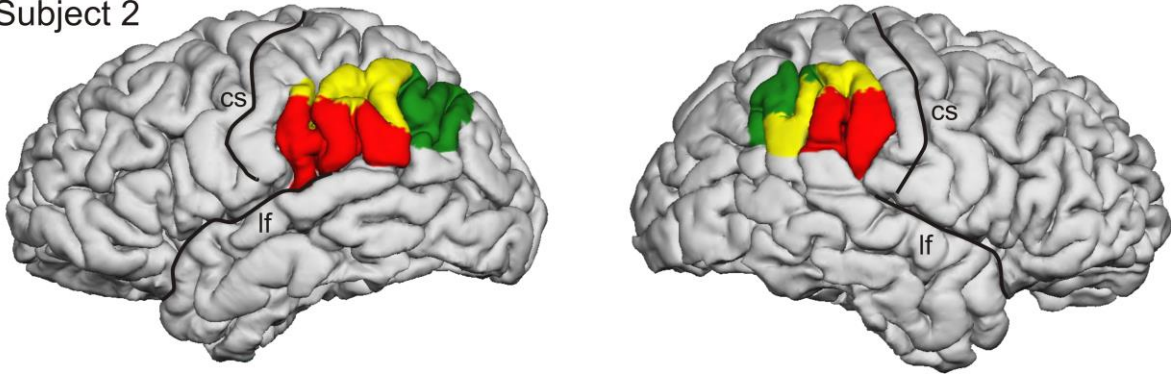
## Results

We varied the number of clusters between 2 and 7 and found 3 to be the maximum number, for which the clusters were compact with a consistent principal spatial arrangement across participants (see *Methods*). More specifically, in 37 out of the 40 tested hemispheres we found 3 compact, and approximately equal-sized regions, in a roughly rostral-caudal arrangement, referred to as inferior parietal cortex anterior (IPCa), IPC middle (IPCm), and IPC posterior (IPCp) (Fig. 3). Fig. 3 also shows the morphometric characterization of the areas in four typical participants (for all participants, see Fig. S1a and Fig. S1b in the supplementary data).

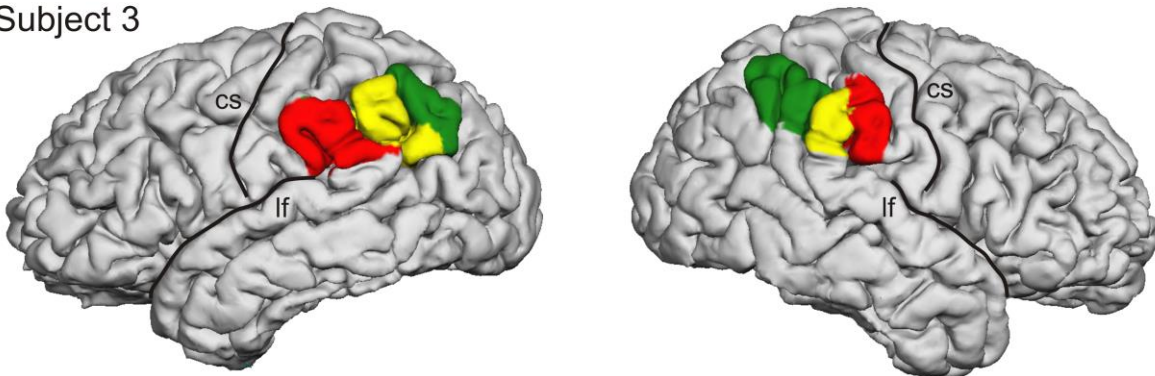
Subject 1



Subject 2



Subject 3



Subject 4

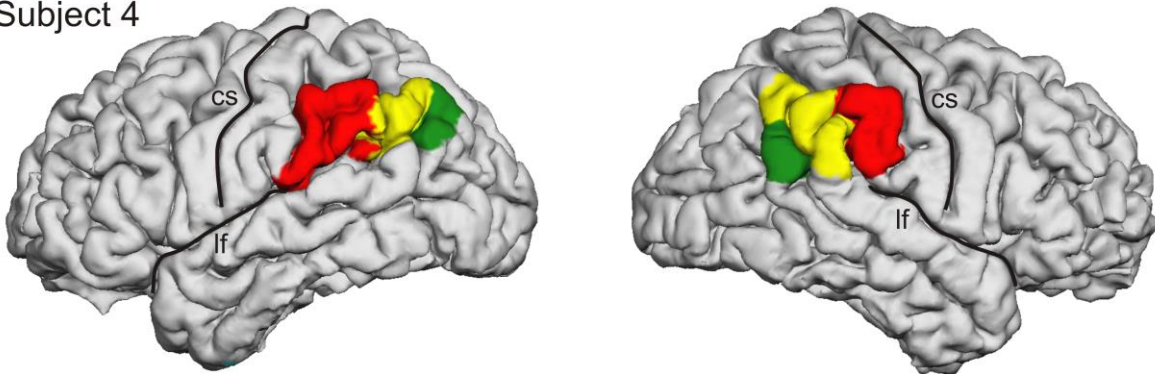
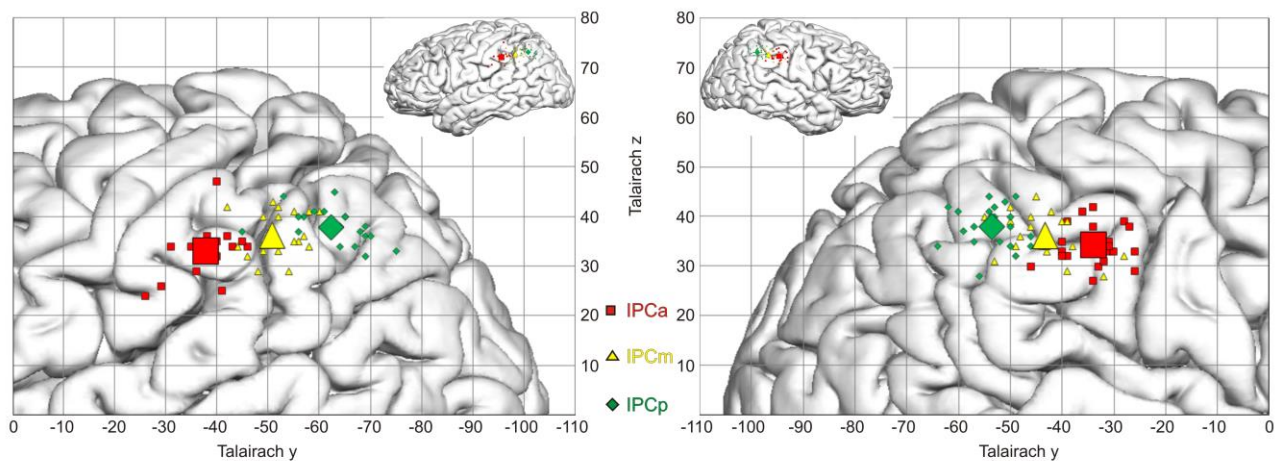


Fig. 3. Parcellations of the left and right IPCC of four representative participants into IPCa (red), IPCm (yellow), and IPCp (green) superimposed on a 3D reconstruction of the pial surface; cs = central sulcus; lf = lateral fissure.

The variability and reproducibility of the parcellation results of all participants is represented by the centers of mass of sub-areas (Fig. 4). From Fig. 4, one can see that IPCa mainly coincides with the supramarginal gyrus (roughly BA 40), while IPCp maps onto the angular gyrus (BA 39). Area IPCm is located in the transition area between the two gyri. The IPCCs of the left and right hemispheres (as well as the corresponding sub-areas) were found to have similar sizes (Fig. 4). Comparing the sizes of the sub-areas across hemispheres, we found similar sized IPCm and IPCp and a slightly bigger IPCa. The size of the sub-areas was measured by counting the number of boundary voxels at the grey-white matter interface. This number was converted into  $\text{cm}^2$  representing the size of each areas folded surface. The centers of mass of the sub-areas show a consistent rostro-caudal arrangement across participants. In the right hemisphere the regions are located slightly more anteriorly. The variability of the spatial location across participants is comparable for all sub-areas (see standard deviations in Fig. 4).



	Mean size		Mean center-of-mass coordinates		
	Size ( $\text{cm}^2$ )	SD ( $\text{cm}^2$ )	x $\pm$ SD	y $\pm$ SD	z $\pm$ SD
Left hemisphere	37.8	9.4			
IPC a	15.7 (41 %)	4.7	-51.1 $\pm$ 2.1	-37.9 $\pm$ 5.0	33.0 $\pm$ 4.8
IPC m	11.6 (31 %)	4.2	-45.2 $\pm$ 4.2	-50.8 $\pm$ 6.4	36.2 $\pm$ 4.6
IPC p	10.6 (28 %)	4.0	-38.1 $\pm$ 3.6	-62.3 $\pm$ 7.5	37.9 $\pm$ 3.5
Right hemisphere	38.3	6.4			
IPC a	14.1 (37 %)	4.9	48.6 $\pm$ 3.6	-33.9 $\pm$ 5.5	34.2 $\pm$ 4.1
IPC m	12.3 (32 %)	3.2	46.2 $\pm$ 3.6	-43.3 $\pm$ 6.9	36.2 $\pm$ 4.4
IPC p	11.9 (31 %)	4.7	40.2 $\pm$ 3.4	-53.6 $\pm$ 5.1	37.9 $\pm$ 4.4

Fig. 4. Top: Illustrating the centers-of-mass of IPCa (red), IPCm (yellow) and IPCp (green) in the left (left) and right (right) hemispheres superimposed on the Talairach coordinate system. Small symbols represent the center-of-mass of each individual subject and large symbols are the mean center-of-mass across all participants. Bottom: Size (in  $\text{cm}^2$  with standard deviation, SD) and locations (in Talairach coordinates) of the different IPC sub-areas.

Fig. 5 shows the population maps illustrating the variability of the computed IPCC sub-areas over participants displayed on the single subject MNI standard brain. The strong overlap of the population map across subjects shows the consistency of the subdivision into 3 areas. The agreement was best for the IPCa area. Left and right hemispheres show similar results.

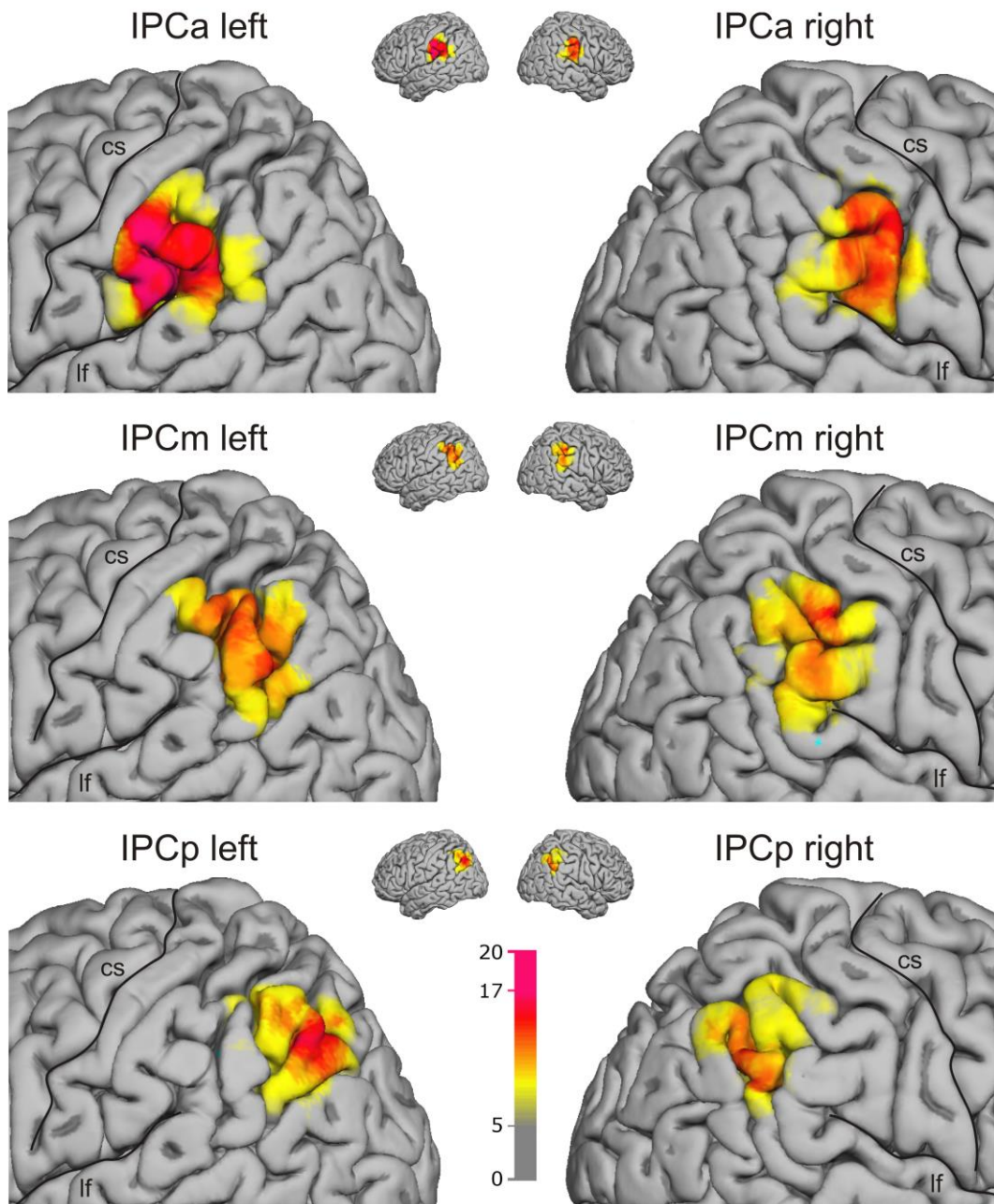


Fig. 5. Population maps ( $n = 20$  brains, cf. color bar) of areas IPCa (top), IPCm (middle), and IPCp (bottom) superimposed on the MNI single subject brain; cs = central sulcus; lf = lateral fissure. Voxels that belong to the respective area in less than 5 participants are not shown.

The full 3D population maps in MNI space of all IPCC areas are publicly available<sup>5</sup> and additionally provided as supplementary data (S3), which can be used with functional imaging software packages such as FSLView or SPM.

Fig. 6 shows, for each IPCC sub-area, the group average of the connectivity, as quantified by the tractographic signature value in the grey-white matter interface. This representation provides a high resolution overview on the connectivity profiles of the areas. The connectivity patterns show a strong overlap between areas, but there are also some substantial differences. For example, connections to ventral premotor cortex are stronger for anterior as compared to posterior regions, and connections to the temporal lobe are stronger in the left hemisphere than in the right. This illustration of the mean tractogram on the inflated brain surface (Fig. 6) allows a precise localization of areas connected to the IPCC. Beside local connections to the neighboring parietal and temporal areas all IPCC areas show a long-range connection to the precentral gyrus (PrCG) via the superior longitudinal fascicle (SLF). Additionally a ventral connection to the anterior inferior frontal gyrus (IFG) via the extreme capsule fiber bundle was found for the left IPCp. A slice view of the fiber bundle showing the precise location of the connections within the white matter is provided in the supplementary materials (Fig. S2).

---

<sup>5</sup> <http://openscience.cbs.mpg.de/ipcc>

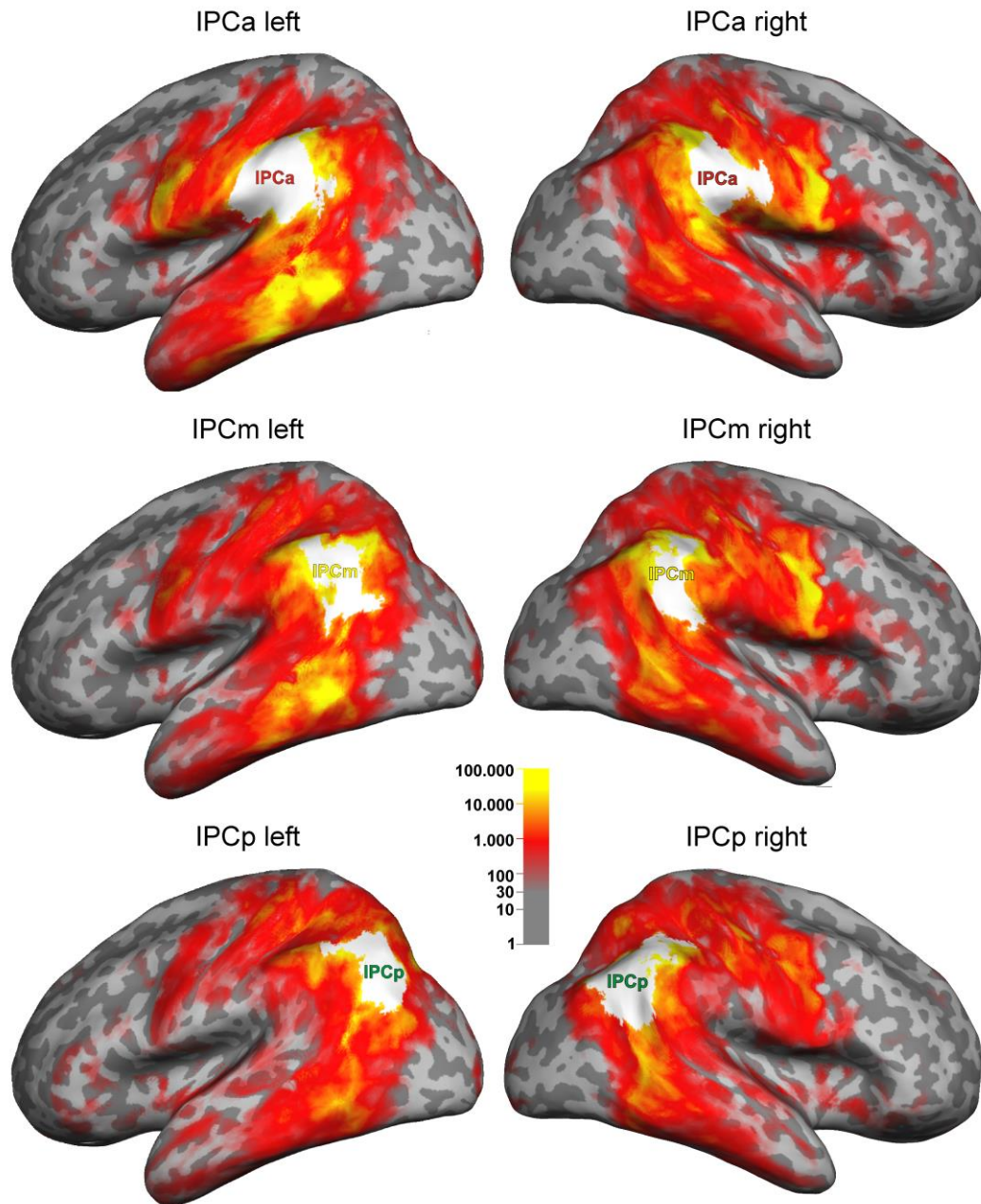


Fig. 6. Group-averaged connectivity of the IPCC sub-areas displayed on an inflated MNI brain. The white areas characterize the average seed areas and are derived from the population maps (see Fig. 5) with a minimum of 5 participants (no overlap between seed regions).

The connection strengths between the IPCC sub-areas and the cortical target regions are depicted in Fig. 7A. Table 1 shows the results of the statistical tests. The strongest connections of areas IPCa, IPCm, and IPCp were found to the lateral temporal cortex (STG, MTG, ITG), the superior parietal cortex (SPL), the pre- and postcentral gyrus (PrCG, PoCG) and the ventro-lateral prefrontal cortex (IFG, MFG; only in the right hemisphere). Connections with the occipital cortex, the dorso-lateral

prefrontal cortex (in both hemispheres) and the ventro-lateral prefrontal cortex (in the left hemisphere) are weaker. There is a significant rostro-caudal (i.e., IPCa-to-IPCp) decrease in connectivity strength to the superior temporal and inferior frontal cortex in the right hemisphere. Moreover, we identified a similar rostral-caudal decrease of connectivity to the superior temporal cortex, and an increase of connectivity to the superior parietal cortex in the left hemisphere (Fig. 7A).

In the left hemisphere we found strong connections to the lateral temporal cortex and the superior parietal cortex and weaker connections to the occipital cortex and lateral frontal cortex. The right hemisphere shows strongest connections to the lateral temporal cortex, superior parietal cortex and lateral frontal cortex. Only sparse connectivity exists to the occipital cortex. Additionally both hemispheres show relatively strong connectivity to the pre- and postcentral gyrus.

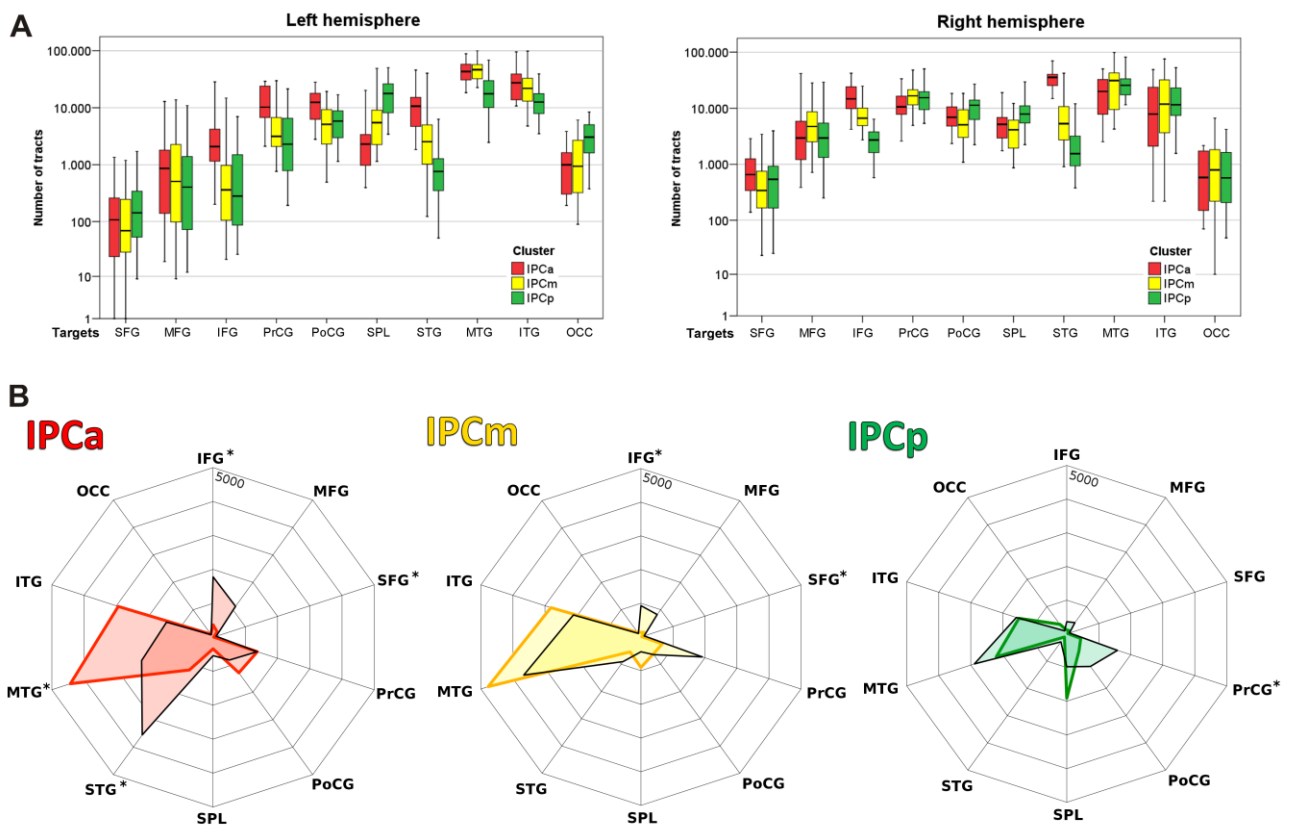


Fig. 7. A: Connectivity between areas IPCa, IPCm, and IPCp and the cortical target regions ( $n = 20$  participants). The box-and-whisker diagrams show the median values, the lower and upper quartiles (boxes), and upper and lower bound (whiskers).

B: Statistical comparison of connectivity fingerprints of IPCC sub-areas between hemispheres. The mean values are indicated by colored lines for the left areas and black lines for the right areas. An asterisk (\*) marks those connections that are significantly different between the hemispheres ( $p < 0.01$ , based on the Wilcoxon test; see *Methods* for details).

Left hemisphere										
	SFG	MFG	IFG	PrCG	PoCG	SPL	STG	MTG	ITG	OCC
Friedmann			***	***	***	***	***	***	*	***
Wilcoxon	IPCa - IPCm		***	***	***	**	***			
	IPCa - IPCp		**	***	***	***	***	**	**	***
	IPCm - IPCp			(*)		**	***	**	*	***

Right hemisphere										
	SFG	MFG	IFG	PrCG	PoCG	SPL	STG	MTG	ITG	OCC
Friedmann			***			**	***			
Wilcoxon	IPCa - IPCm		**				***			
	IPCa - IPCp		***			*	***			
	IPCm - IPCp		***			***	***			

Table 1. Test results for differences between connection strength of IPCC sub-areas. Levels of significance: (\*)  $p < 0.1$  (marginally significant), \*  $p < 0.05$ , \*\*  $p < 0.01$ , \*\*\*  $p < 0.001$ . The p values are Bonferroni corrected for multiple comparisons. See text for details and legend of Fig. 2 for the regions and abbreviations.

To test for significance we performed a two-way repeated measures Friedmann Analysis of Variance (ANOVA) on ranks (factor 1: IPC region; factor 2: target region), followed by a Wilcoxon signed rank test for post hoc pairwise comparisons. The test results show significant differences between IPCa, IPCm, and IPCp in their connectivity strength to the superior temporal cortex and superior parietal cortex. In the right hemisphere, significant differences were also found in the connection strength to the superior temporal cortex and furthermore to the inferior frontal cortex (Fig. 7A and Tab. 1).

Fig. 7B shows the comparison between the connectivity patterns of the corresponding areas in the two hemispheres. In IPCa, the left area has more connections to the MTG, while the right area connects stronger to the STG, SFG and IFG. For the middle area IPCm, the right side has stronger connections to the SFG and IFG. Finally, IPCp shows stronger right side connectivity for the precentral gyrus.

## Discussion

In this study we show that the human inferior parietal cortex convexity (IPCC) can be divided into three sub-areas, arranged in a rostral-caudal direction, with distinct connectivity patterns to the rest of the brain. In addition, the principal topological arrangement and the connectivity patterns of these sub-areas are relatively consistent across participants. The variability between subjects is comparable for all regions and both hemispheres (Fig. 4). Moreover, the connectivity patterns are in principal agreement with previous dMRI based studies of the parietal lobe. For example, connections between rostral IPCC and IFG, as well as ventral premotor and somatosensory areas, have been demonstrated by Rushworth and colleagues (2006), Mars and colleagues (2011) and Caspers and colleagues (2011). While we consistently found for all sub-areas strongest connections to the lateral temporal and superior parietal cortices, there were also striking differences between sub-areas: a rostral-caudal decrease of connection strength to the inferior frontal (only for right hemisphere) and superior temporal regions (both hemispheres), and a rostral-caudal increase of connection strength to the superior parietal cortex (only for left hemisphere)<sup>6</sup>.

### *What is the most appropriate subdivision of the IPCC?*

As with other cortical areas, the exact subdivision of human IPCC has been a matter of debate. For example, Brodmann (1909), on the basis of post-mortem cytoarchitectonics, postulated a subdivision into two areas, while later researchers, even when using the same principal methodology, concluded that there should be a higher number of sub-areas (von Economo and Koskinas 1925; Gerhardt 1940; Sarkissov et al. 1955; Caspers et al. 2006). Recently Caspers and colleagues (2013) used receptor mapping to suggest that the seven cytoarchitectonically defined IPCC sub-areas (Caspers et al., 2006) can be clustered into three larger rostro-caudally arranged regions. Also using post-mortem myeloarchitecture as a structural criterion leads to more than two sub-areas of IPCC (Vogt 1911; Batsch 1956).

The rostral-caudal arrangement found in this study is in agreement with a number of previous studies using cytoarchitecture (e.g., von Economo and Koskinas 1925; Sarkissov et al. 1955; Caspers et al. 2006) and dMRI connectivity (Mars et al. 2011). Concerning the number of

---

<sup>6</sup> Note that it could be argued that the rostral-caudal decreases of connectivity are due to the distance bias associated to probabilistic tractography (Jones 2010). However, as can be seen in Fig. 7A and 7B, the decrease in IFG connectivity from IPCa to IPCp amounts to about a factor between 3 and 5. The upper bound of the distance bias (if fibers spread completely uniformly into all directions) in probabilistic tractography is proportional to the square of the distance. If the diffusion is constrained by coherent structure, this exponent is much lower. Simulations show that it is in the order of 1, which has been used, for example, by Greenberg and colleagues (2012) and Anwender and colleagues (2007). As the distance from IFG to IPCp is less than twice the one from IFG to IPCa (see Fig. 8), the difference in connection strength cannot be purely an effect of distance bias.

distinguishable areas, however, there are differences. Mars and colleagues (2011) subdivided, at least, the right IPCC into five rostro-caudally arranged areas, consistently over several participants. Here, we must consider two facts. First, these authors used a large region of interest that included both the parietal operculum (indeed, one of the five clusters was mainly located there) and anterior parts of the occipital lobe. Second, Mars and colleagues did not only rely on anatomical connectivity for parcellation, but additionally asked for compact clusters. This additional assumption might have stabilized the parcellation and allowed for a higher number of sub-areas to be consistent across participants. Caspers and colleagues (2006) found seven cytoarchitecturally defined rostro-caudally arranged areas altogether. However, they also acknowledge that neighboring areas tend to be similar and can be combined (cytoarchitectonic gradient).

So, it seems that the anatomical similarity structure of the cortex across studies in the field does not converge to a clear distinction into a fixed number of homogeneous and clearly distinguishable areas. Instead, it appears that the number, location, and precise boundaries of areas are a matter of: (i) the structural traits used as parcellation criteria (e.g., cytoarchitecture or long-range connectivity) and the sensitivity of the methodology to extract them, and (ii) the level of detail considered relevant for the particular researchers (i.e., the desired granularity of the parcellation). With respect to the former point, one may conclude that an exact agreement between the earlier results based on cortical microstructure and our findings based on long-range connectivity profiles, is neither necessary nor likely. Concerning the latter point, the question remains: How many sub-areas of the IPCC would represent the most appropriate parcellation? Here we argue that it is sensible to choose the most detailed description (i.e., the largest number of areas) that still leads to a consistent pattern across participants. Any attempt to produce finer parcellations would highlight inter-individual differences, while any coarser subdivision would miss potentially relevant features. The remaining variability of cluster size and location might be a source to study the individual arrangement of functional zones in the IPC. Based on these considerations, the criterion of long-range connectedness and using the current technology to characterize this connectedness, we suggest that a subdivision of the IPCC into three areas is the most appropriate.

### ***Connectivity pattern of the human IPCC***

This study shows strongest connections of the IPCC to the lateral temporal, superior parietal, pre- and postcentral cortex in both hemispheres. The IPCC sub-areas are characterized by a significant rostral-caudal (i.e., IPCa-to-IPCp) decrease and increase in particular connectivity patterns to certain cortical areas. A connectivity decrease from rostral to caudal was identified to the superior

temporal cortex in both hemispheres, and an increase to the superior parietal cortex in the left hemisphere.

In agreement with the study from Caspers and colleagues (2011) we identified the strongest connections between all IPCC sub-areas and the temporal cortex. We also found a comparable connectivity pattern in the left and right hemisphere. On the other hand some of the rostral-caudal connectivity gradients of the current work differ from the study of Caspers and colleagues, in which for example rostral areas are more connected to somatosensory and superior parietal areas while caudal areas are predominantly connected to auditory, anterior temporal and occipital cortex. The connections patterns are not directly comparable due to differences in the methodology to compute the connectivity values from diffusion tractography. However, the main difference consists in the definition of seed and target regions. While we used the voxels at the grey-white matter interface in the entire IPCC sub-areas as seed region, Caspers and colleagues used a small area representing the top 10% of the maximum probability map (Caspers 2008) and computed the connectivity values to a small target zones within the target areas. Further on, their measures are based on the connection likelihood and not on the connection strength computed by probabilistic tractography.

### ***Methodological considerations***

The measured diffusion signal is only an indirect measure of the brain microstructure and therefore the derived tractography does not directly reflect the fine details of anatomical connectivity (Jones et al. 2012). Some of the computed connections might not exist in the brain (false positive connections) and the method cannot capture the full connectivity of the brain (false negative connections). The estimated connectivity values do not represent the true axonal fiber-count in the living brain and is only a relative measure of linkage between regions. Nevertheless the computed estimation of the long-range connectivity is a powerful criterion to separate cortical areas with different connectivity, even if definite connectivity remains unknown. Despite these limitations diffusion tractography provides relevant information of the white matter connectivity as shown in numerous studies (e.g. Assaf and Pasternak 2008).

### ***Homology – comparison to monkey data***

Besides having optimal consistency across participants, the proposed subdivision of human IPCC into three sub-areas arranged in rostral-caudal direction, is also supported by its similarity to the subdivision of the macaque IPCC (areas PF, PFG, and PG), according to studies of cytoarchitecture (Gregoriou et al. 2006), tract tracing (Rozzi et al. 2006), and electrophysiology (Rozzi et al. 2008).

The small area Opt, the fourth area in the macaque IPCC, which is located on the boundary to the occipital lobe markedly differs from the other IPCC areas in terms of cytoarchitecture and connectivity (Pandya et al., 1982; Rozzi et al., 2006) and is not clearly associated to the parietal lobe. We therefore excluded this area from the comparative analysis.

The next question is whether the human and the macaque areas are comparable with respect to their connectivity patterns and whether there are any important differences between the two species. In the macaque, areas PF, PFG, and PG are connected with the lateral premotor cortex (area F4 and F5) and the intraparietal and superior parietal cortices via the superior longitudinal fasciculus (SLF) II/III (Rozzi et al. 2006; Schmahmann and Pandya 2006). Similarly, in humans, areas IPCa, IPCm, and IPCp are connected with the inferior frontal gyrus (containing Brodmann area 44, the presumed human homologue of macaque area F5) and the superior parietal cortex. These similarities in parieto-frontal connections are also corroborated in a recent study by Thiebaut de Schotten et al. (2011), who demonstrated a striking similarity between the architecture of the SLF in macaques and in humans.

In addition to these similarities there are also clear differences (Fig. 8). In monkeys, only sparse connections seem to exist between the IPCC and the temporal cortex (see Seltzer and Pandya 1984; Fig. 8; Rozzi et al. 2006; Schmahmann et al. 2007). In marked contrast to that, in humans strong connections exist between all three regions of the IPCC and the lateral temporal cortex. These connections follow the posterior, vertical section of the arcuate fascicle (Catani et al. 2005)<sup>7</sup>. Additionally, tractography revealed strong connectivity of all three regions with the pre- and post-central gyrus. These connections were not described in this extend in the macaque monkey.

The similarity in IPCC parcellation between macaques and humans and the similar connections between the IPCC and frontal and parietal regions suggests substantial conservation in IPCC evolution between the two primate species. However, in humans, new structural features emerged, such as the pronounced pathway between the IPCC and temporal cortex, which is possibly part of a perisylvian language network of the human brain (Catani et al. 2005; Schmahmann et al. 2007; Friederici 2009).

---

<sup>7</sup>Connections to deep white matter structures (e.g., the long segment of the arcuate fascicle) were excluded by carefully selecting the seed region at the cortical interface (see *Methods*).

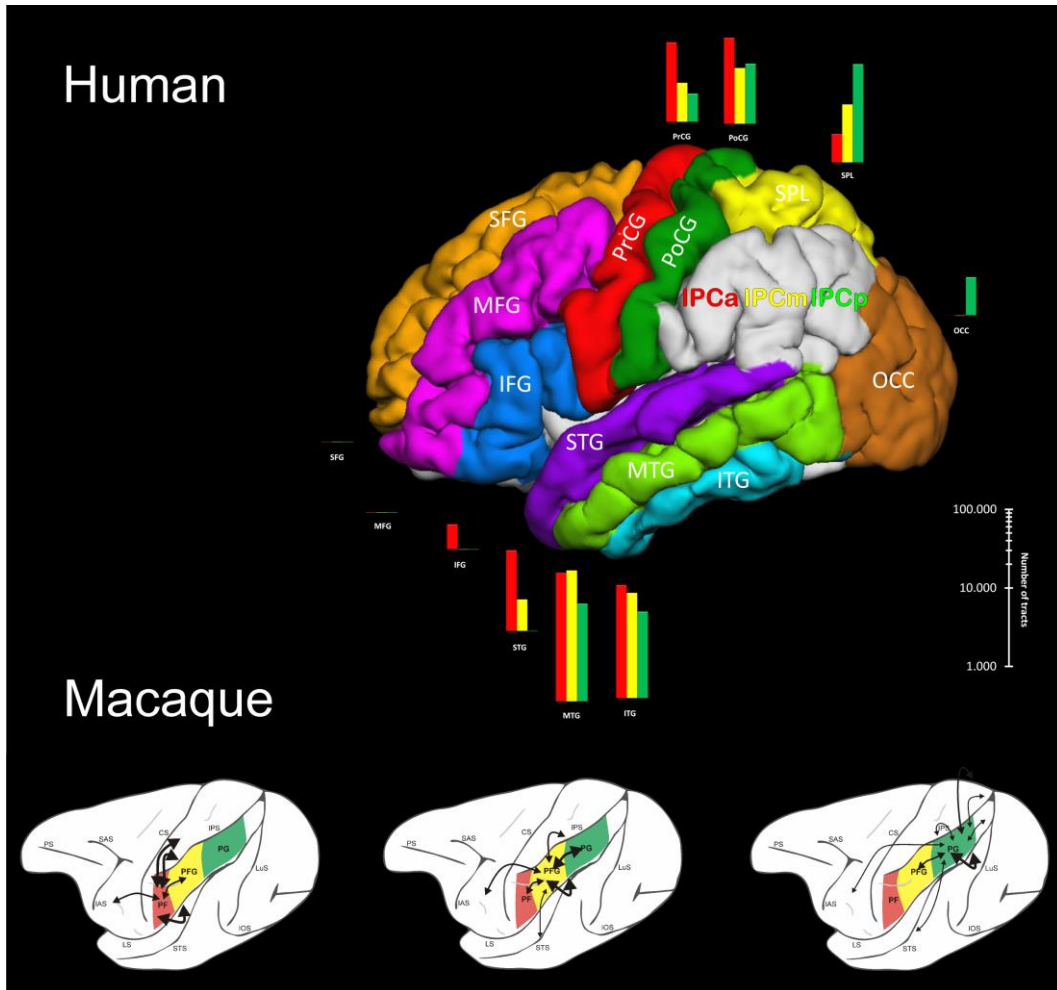


Fig. 8. Parcellation and connectivity strengths of IPCa (red), IPCm (yellow), IPCp (green) with other regions in human (top) compared to PF, PFG, PG in macaque (bottom) ("classical" tract tracing data in the macaque from Rozzi et al., 2006).

### *The functional relevance of the IPCC parcellation*

As discussed in the *Introduction*, sub-areas of the IPCC are involved in several important cognitive networks, including those subserving language, spatial attention and episodic memory. These networks have been investigated in numerous functional brain imaging studies. We will now discuss how the sub-areas we have found on the basis of tractography, as well as the associated connectional fingerprints, might relate to these functional findings. Similar to Caspers and colleagues (2006), we consider IPCm to be a transition area between the rostral (IPCa) and caudal (IPCp) subregions of the IPCC, and IPCa and IPCp as transition area to other cortical regions.

#### *Rostral IPCC*

The sub-area IPCa covers the rostral part of the IPCC and largely corresponds to supramarginal gyrus. This area has been interpreted to be involved in phonological processing (Obleser et al.

2006) and, together with the dorsal part of the IFG, in phonological working memory (Vigneau et al. 2006). Similarly, the area was found active for phonology-orthography mapping (Graves et al. 2010), phonological decision (Hartwigsen et al. 2010) and subvocal articulation (Price 2010). This phonological network comprises, besides bilateral IPCa and the IFG, posterior MTG and fusiform gyrus (Graves et al. 2010). In contrast to these phonological findings, other language functions seem to markedly exclude rostral IPCC (Vigneau et al. 2006).

Furthermore, although lesions in the posterior parietal cortex do not usually cause gross memory deficits, imaging studies have shown that the region is involved in episodic memory (Cabeza et al. 2008). In particular, familiarity based episodic memory effects are primarily found in supramarginal gyrus (Vilberg and Rugg 2008).

Finally, rostral IPCC seems to store abstract somatosensory information associated with tool use and complex movements (Binder et al. 2009). Hence, it should be in close connection with other motor and somatosensory areas, such as on the pre- and postcentral gyri. Indeed, Rizzolatti and colleagues (2004) have shown that the rostral IPCC belongs to the mirror neuron network and is activated during imitation and observation of actions (see also Caspers et al. 2010). Also, in these studies it was shown that rostral IPCC coactivates with pre-motor and somatosensory cortices.

Similar networks to the ones found by the experiments described above also seem to emerge from resting state fMRI studies (e.g., Kelly et al. 2010).

In our analysis, we found substantial connections between IPCa and all tested target regions. However, the regions most strongly connected to IPCa comprise the IFG, pre- and postcentral gyri, as well as the temporal lobe (ITG, MTG and STG). This network includes, but is not limited to, the functionally connected areas discussed above (note that fusiform gyrus was not tested here).

Comparing the connection strength between the hemispheres, we first find a right lateralization of connections between IPCa and prefrontal (IFG and SFG), as well as superior temporal (STG) areas. While the frontal connections fit well with a right lateralized visio-spatial attention network (Umarova et al. 2011), the meaning of the strongly right lateralized STG and the strongly left lateralized MTG connections remains somewhat unclear.

### *Caudal IPCC*

The caudal sub-area of the IPCC identified in our analysis (IPCp) lies on the angular gyrus. The area has been discussed as supporting semantic processes (Humphries et al. 2007) and, together

with parts of the IFG, to be involved in semantic working memory (for a review see Vigneau et al. 2006).

In studies of visiospatial attention, besides the dorsal attention network which subserves goal directed attention, a ventral bottom-up attention network has been discovered that underlies direction of attention towards salient stimuli and acts as a ‘circuit breaker’ for the dorsal network (Corbetta and Shulman 2002). This network recruits mainly angular gyrus, as well as the posterior parts of MFG and IFG.

More generally, it seems that the caudal part of the IPCC houses neuronal populations that are involved in processes of high-level, complex and supramodal integration, such as decision making, planning, problem solving and sentence comprehension (Binder et al. 2009).

In our study, the sub-areas IPCm and IPCp are also principally connected to all target areas. However, some areas are particularly strongly connected, such as left SPL. This fits with the idea that this area has special involvement in networks of episodic memory and spatial attention (Corbetta and Shulman 2002; Cabeza et al. 2008). On the other hand, IPCm and IPCp are also strongly connected with temporal areas of the language network, thus corroborating their involvement in language comprehension (Vigneau et al. 2006).

Concerning the inter-hemispheric differences between the connections of caudal IPCC we find that in the right hemisphere there are stronger connections to the precentral gyrus (more posteriorly, IPCp), and to IFG/SFG (more anteriorly, IPCm). This connection pattern bears a striking resemblance to the SLF III system (see Schmahmann et al. 2007), a fiber system whose right lateralization has been shown to correlate to performance in visio-spatial attention tasks (Thiebaut de Schotten et al. 2011).

## **Conclusions**

Our connectivity based tripartition of the human inferior parietal cortex convexity (IPCC) as well as the associated connectivity patterns are in principal agreement with previous studies, both, based on diffusion tractography and invasive methods. We extend the earlier work in several ways. First, we provide direct insight into the inter-subject variability of the parcellation. These data are also provided as an atlas in the supplementary data (S3). Second, we directly assess the lateralization of parcellation and connectivity fingerprints of the sub-areas. While the parcellation showed only slight inter-hemispheric differences, the associated connections are markedly different: in contrast to the left hemisphere, the right anterior IPCC features stronger prefrontal and superior temporal

connectivity, posterior IPCC is stronger connected to superior parietal and prefrontal areas. Third, we compare and extensively discuss the relationship between our findings in humans and previous tracing work in monkeys. While the rostro-caudal arrangement of the sub-areas is similar to the findings in the macaque, the connectivity patterns bear important differences, in that, humans in contrast to the monkeys have strong connections between IPCC and temporal cortex, possibly related to the human ability to process language. In summary, this study gives a more complete picture of the structure of the IPCC and provides a blueprint for similar investigations of other regions of the cortex.

## **Funding**

This work was supported by a University Leipzig MD Grant to M.R. and the Future and Emerging Technologies (FET) project CONNECT of the European Union, under FET-Open grant number: 238292: <http://www.brain-connect.eu>.

## **Acknowledgements**

We thank Tania Douglas for valuable technical advice.

## References

- Anwander A, Tittgemeyer M, von Cramon DY, Friederici AD, Knösche TR. 2007. Connectivity-based parcellation of Broca's area. *Cereb Cortex*. 17:816-825.
- Assaf Y, Pasternak O. 2008. Diffusion tensor imaging (DTI)-based white matter mapping in brain research: A review. *J Mol Neurosci*. 34:51-61.
- Basser PJ, Mattiello J, LeBihan D. 1994. Estimation of the effective self-diffusion tensor from the NMR spin echo. *J Magn Reson B*. 103:247-254.
- Batsch E. 1956. Die myeloarchitektonische Untergliederung des Isocortex parietalis beim Menschen. *J Hirnforsch*. 2:259-270.
- Beckmann M, Johansen-Berg H, Rushworth MF. 2009. Connectivity-based parcellation of human cingulate cortex and its relation to functional specialization. *J Neurosci*. 29:1175-1190.
- Behrens TEJ, Johansen-Berg H, Woolrich MW, Smith SM, Wheeler-Kingshott CAM, Boulby PA, Barker GJ, Sillery EL, Sheehan K, Ciccarelli O, Thompson AJ, Brady JM, Matthews PM. 2003. Non-invasive mapping of connections between human thalamus and cortex using diffusion imaging. *Nat Neurosci*. 6:750-757.
- Binder JR, Desai RH, Graves WW, Conant LL. 2009. Where is the semantic system? A critical review and meta-analysis of 120 functional neuroimaging studies. *Cereb Cortex*. 19:2767-2796.
- Brodmann K. 1909. *Vergleichende Lokalisationslehre der Großhirnrinde*. Leipzig: Barth.
- Cabeza R, Ciaramelli E, Olson IR, Moscovitch M. 2008. The parietal cortex and episodic memory: an attentional account. *Nat Rev Neurosci*. 9:613-625.
- Caspers S, Eickhoff SB, Geyer S, Scheperjans F, Mohlberg H, Zilles K, Amunts K. 2008. The human inferior parietal lobule in stereotaxic space. *Brain Struct Funct*. 212:481-495.
- Caspers S, Eickhoff SB, Rick T, von Kapri A, Kuhlen T, Huang R, Shah NJ, Zilles K. 2011. Probabilistic fibre tract analysis of cytoarchitectonically defined human inferior parietal lobule areas reveals similarities to macaques. *Neuroimage*. 58:362-380.
- Caspers S, Geyer S, Schleicher A, Mohlberg H, Amunts K, Zilles K. 2006. The human inferior parietal cortex: Cytoarchitectonic parcellation and interindividual variability. *Neuroimage*. 33:430-448.

- Caspers S, Schleicher A, Bacha-Trams M, Palomero-Gallagher N, Amunts K, Zilles K. 2013. Organization of the human inferior parietal lobule based on receptor architectonics. *Cereb Cortex* 23:615-628.
- Caspers S, Zilles K, Laird AR, Eickhoff SB. 2010. ALE meta-analysis of action observation and imitation in the human brain. *Neuroimage*. 50:1148-1167.
- Catani M, Jones DK, Ffytche DH. 2005. Perisylvian language networks of the human brain. *Ann Neurol*. 57:8-16.
- Choi HJ, Zilles K, Mohlberg H, Schleicher A, Fink GR, Armstrong E, Amunts K. 2006. Cytoarchitectonic identification and probabilistic mapping of two distinct areas within the anterior ventral bank of the human intraparietal sulcus. *J Comp Neurol*. 495:53-69.
- Corbetta M, Shulman GL. 2002. Control of goal-directed and stimulus-driven attention in the brain. *Nat Rev Neurosci*. 3:201-215.
- Fischl B, Sereno MI, Dale AM. 1999. Cortical surface-based analysis. II: Inflation, flattening, and a surface-based coordinate system. *Neuroimage*. 9:195-207.
- Friederici AD. 2009. Pathways to language: fiber tracts in the human brain. *Trends Cogn Sci*. 13:175-181.
- Gerhardt E. 1940. Die Cytoarchitektonik des Isocortex parietalis beim Menschen. *J Psychol Neurol*. 49:367-419.
- Geyer S, Luppino G, Ekamp H, Zilles K. 2005. The macaque inferior parietal lobule: Cytoarchitecture and distribution pattern of serotonin 5-HT 1A binding sites. *Anat Embryol*. 210:353-362.
- Gorbach NS, Schutte C, Melzer C, Goldau M, Sujazow O, Jitsev J, Douglas T, Tittgemeyer M. 2011. Hierarchical information-based clustering for connectivity-based cortex parcellation. *Front Neuroinform*. 5:18.
- Graves WW, Desai R, Humphries C, Seidenberg MS, Binder JR. 2010. Neural systems for reading aloud: a multiparametric approach. *Cereb Cortex*. 20:1799-1815.
- Greenberg AS, Verstynen T, Chiu YC, Yantis S, Schneider W, Behrmann M. 2012. Visuotopic cortical connectivity underlying attention revealed with white-matter tractography. *J Neurosci*. 32:2773-2782.
- Gregoriou GG, Borra E, Matelli M, Luppino G. 2006. Architectonic organization of the inferior parietal convexity of the macaque monkey. *J Comp Neurol*. 496:422-451.

- Hartwigsen G, Baumgaertner A, Price CJ, Koehnke M, Ulmer S, Siebner HR. 2010. Phonological decisions require both the left and right supramarginal gyri. *Proc Natl Acad Sci U S A*. 107:16494-16499.
- Humphries C, Binder JR, Medler DA, Liebenthal E. 2007. Time course of semantic processes during sentence comprehension: an fMRI study. *Neuroimage*. 36:924-932.
- Jenkinson M, Bannister P, Brady M, Smith S. 2002. Improved optimization for the robust and accurate linear registration and motion correction of brain images. *Neuroimage*. 17:825-841.
- Johansen-Berg H, Behrens TEJ, Robson MD, Drobnjak I, Rushworth MFS, Brady JM, Smith SM, Higham DJ, Matthews PM. 2004. Changes in connectivity profiles define functionally distinct regions in human medial frontal cortex. *Proc Natl Acad Sci U S A*. 101:13335-13340.
- Johansen-Berg H, Behrens TEJ, Sillery E, Ciccarelli O, Thompson AJ, Smith SM, Matthews PM. 2005. Functional-anatomical validation and individual variation of diffusion tractography-based segmentation of the human thalamus. *Cereb Cortex*. 15:31-39.
- Jones DK. 2010. Challenges and limitations of quantifying brain connectivity in vivo with diffusion MRI. *Imag Med*. 2:341-355.
- Jones DK, Knösche TR, Turner R. 2012. White matter integrity, fiber count, and other fallacies: The do's and don'ts of diffusion MRI. *Neuroimage*. doi: 10.1016/j.neuroimage.2012.06.081.
- Kelly C, Uddin LQ, Shehzad Z, Margulies DS, Castellanos FX, Milham MP, Petrides M. 2010. Broca's region: linking human brain functional connectivity data and non-human primate tracing anatomy studies. *Eur J Neurosci*. 32:383-398.
- Klein JC, Behrens TEJ, Robson MD, Mackay CE, Higham DJ, Johansen-Berg H. 2007. Connectivity-based parcellation of human cortex using diffusion MRI: Establishing reproducibility, validity and observer independence in BA 44/45 and SMA/pre-SMA. *Neuroimage*. 34:204-211.
- Mars RB, Jbabdi S, Sallet J, O'Reilly JX, Crosson PL, Olivier E, Noonan MP, Bergmann C, Mitchell AS, Baxter MG, Behrens TE, Johansen-Berg H, Tomassini V, Miller KL, Rushworth MF. 2011. Diffusion-weighted imaging tractography-based parcellation of the human parietal cortex and comparison with human and macaque resting-state functional connectivity. *J Neurosci*. 31:4087-4100.

- Obleser J, Boecker H, Drzezga A, Haslinger B, Hennenlotter A, Roettinger M, Eulitz C, Rauschecker JP. 2006. Vowel sound extraction in anterior superior temporal cortex. *Hum Brain Mapp.* 27:562-571.
- Ono M, Kubik S, Abernathy CD. 1990. *Atlas of the Cerebral Sulci*. Stuttgart: Thieme.
- Pandya DN, Seltzer B. 1982. Intrinsic connections and architectonics of posterior parietal cortex in the rhesus monkey. *J Comp Neurol.* 204:196-210.
- Price CJ. 2010. The anatomy of language: a review of 100 fMRI studies published in 2009. *Ann N Y Acad Sci.* 1191:62-88.
- Rizzolatti G, Craighero L. 2004. The mirror-neuron system. *Annu Rev Neurosci.* 27:169-192.
- Rozzi S, Calzavara R, Belmalih A, Borra E, Gregoriou GG, Matelli M, Luppino G. 2006. Cortical connections of the inferior parietal cortical convexity of the macaque monkey. *Cereb Cortex.* 16:1389-1417.
- Rozzi S, Ferrari PF, Bonini L, Rizzolatti G, Fogassi L. 2008. Functional organization of inferior parietal lobule convexity in the macaque monkey: Electrophysiological characterization of motor, sensory and mirror responses and their correlation with cytoarchitectonic areas. *Eur J Neurosci.* 28:1569-1588.
- Rushworth MFS, Behrens TEJ, Johansen-Berg H. 2006. Connection patterns distinguish 3 regions of human parietal cortex. *Cereb Cortex.* 16:1418-1430.
- Sakai KL, Hashimoto R, Homae F. 2001. Sentence processing in the cerebral cortex. *Neurosci Res.* 39:1-10.
- Sarkissov SA, Filimonoff IN, Kononowa EP, Preobraschenskaja IS, Kukuw LA. 1955. *Atlas of the Cytoarchitectonics of the Human Cerebral Cortex*. Moscow: Medgiz.
- Schleicher A, Amunts K, Geyer S, Morosan P, Zilles K. 1999. Observer-independent method for microstructural parcellation of cerebral cortex: A quantitative approach to cytoarchitectonics. *Neuroimage.* 9:165-177.
- Schmahmann JD, Pandya DN. 2006. *Fiber Pathways of the Brain*. Oxford: Oxford University Press.
- Schmahmann JD, Pandya DN, Wang R, Dai G, D'Arceuil HE, de Crespigny AJ, Wedeen VJ. 2007. Association fibre pathways of the brain: Parallel observations from diffusion spectrum imaging and autoradiography. *Brain.* 130:630-653.
- Schubotz RI, Anwender A, Knösche TR, von Cramon DY, Tittgemeyer M. 2010. Anatomical and functional parcellation of the human lateral premotor cortex. *Neuroimage.* 50:396-408.

- Seltzer B, Pandya DN. 1984. Further observations on parieto-temporal connections in the rhesus monkey. *Exp Brain Res.* 55:301-312.
- Thiebaut de Schotten M, Dell'Acqua F, Forkel SJ, Simmons A, Vergani F, Murphy DG, Catani M. 2011. A lateralized brain network for visuospatial attention. *Nat Neurosci.* 14:1245-1246.
- Tomassini V, Jbabdi S, Klein JC, Behrens TEJ, Pozzilli C, Matthews PM, Rushworth MFS, Johansen-Berg H. 2007. Diffusion-weighted imaging tractography-based parcellation of the human lateral premotor cortex identifies dorsal and ventral subregions with anatomical and functional specializations. *J Neurosci.* 27:10259-10269.
- Umarova RM, Saur D, Kaller CP, Vry MS, Glauche V, Mader I, Hennig J, Weiller C. 2011. Acute visual neglect and extinction: distinct functional state of the visuospatial attention system. *Brain.* 134:3310-3325.
- Vigneau M, Beaucousin V, Herve PY, Duffau H, Crivello F, Houde O, Mazoyer B, Tzourio-Mazoyer N. 2006. Meta-analyzing left hemisphere language areas: phonology, semantics, and sentence processing. *Neuroimage.* 30:1414-1432.
- Vilberg KL, Rugg MD. 2008. Memory retrieval and the parietal cortex: a review of evidence from a dual-process perspective. *Neuropsychologia.* 46:1787-1799.
- Vogt C, Vogt O. 1919. Allgemeine Ergebnisse unserer Hirnforschung. *J Psychol Neurol.* 25:279-461.
- Vogt O. 1911. Die Myeloarchitektonik des Isocortex parietalis. *J Psychol Neurol.* 18:379-390.
- von Bonin G, Bailey P. 1947. *The Neocortex of Macaca Mulatta.* Urbana, Illinois: University of Illinois Press.
- von Economo K, Koskinas G. 1925. *Die Cytoarchitektonik der Hirnrinde des erwachsenen Menschen.* Wien: Springer.

## Supplementary Material 1

To manuscript: “Connectivity architecture and subdivision of the human inferior parietal cortex revealed by diffusion MRI”

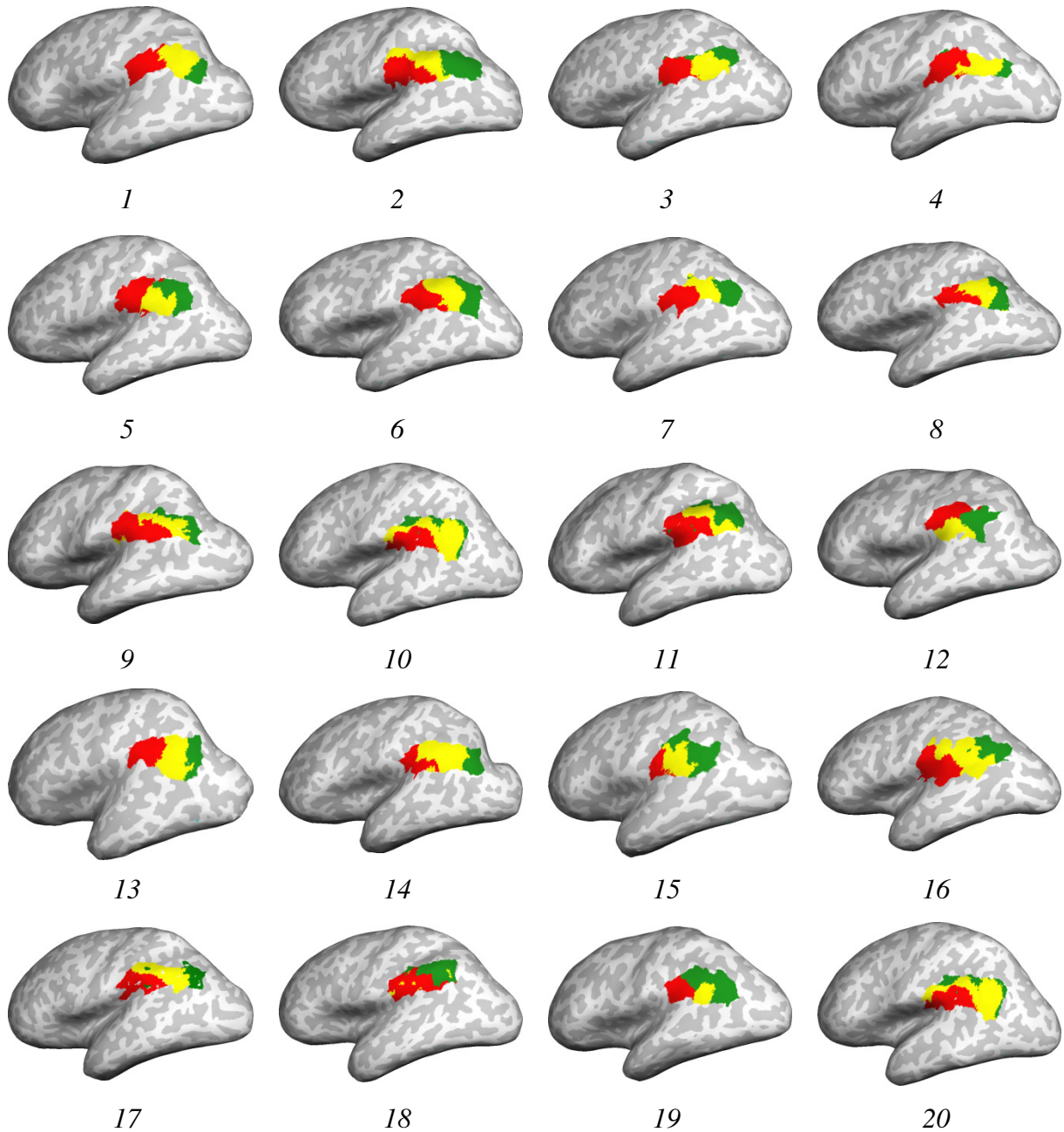


Figure S1a: Parcellations of the left IPCC.

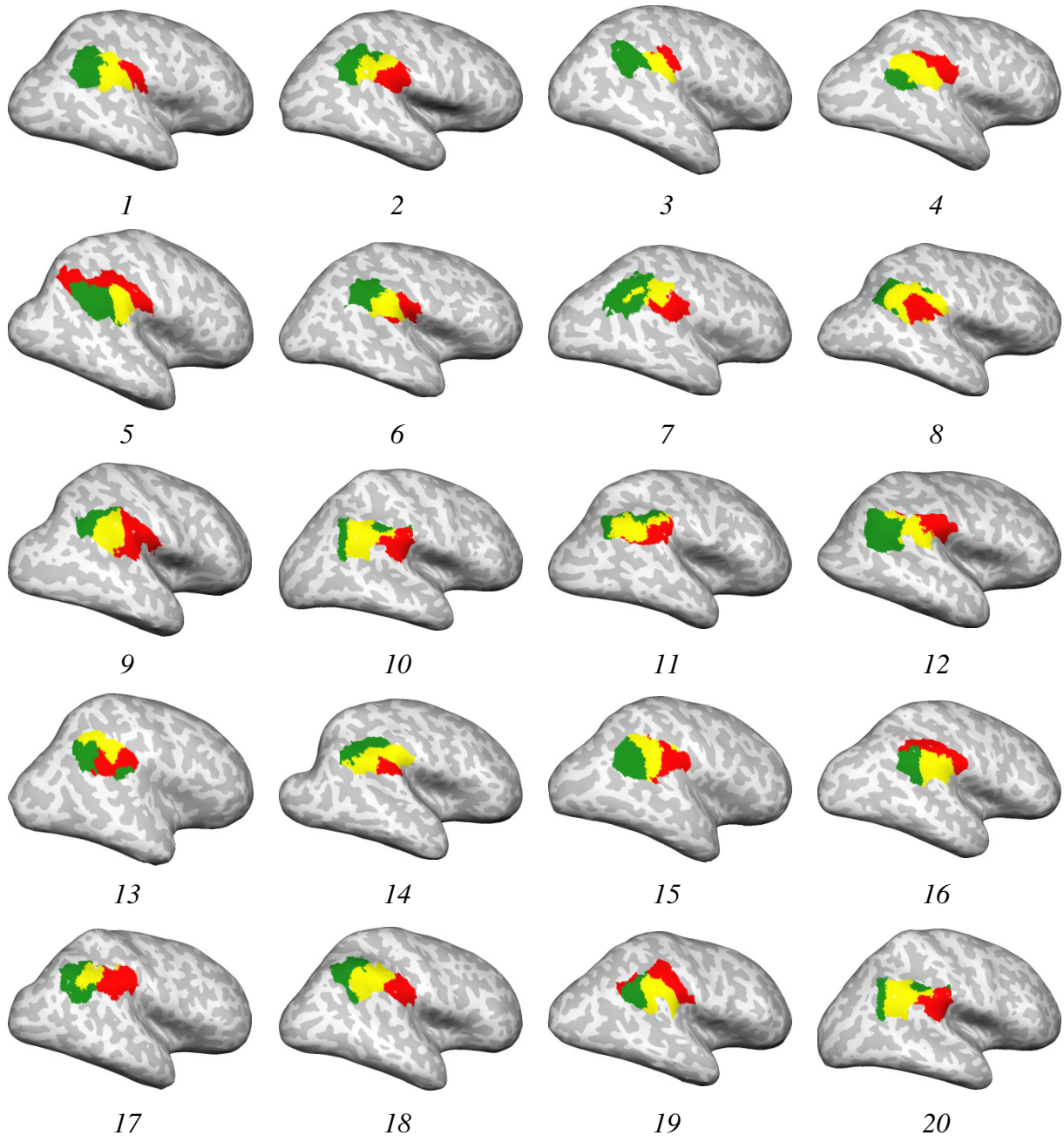


Figure S1b: Parcellations of the right IPCC.

Supplementary Material (2)

To manuscript: “Connectivity architecture and subdivision of the human inferior parietal cortex revealed by diffusion MRI”

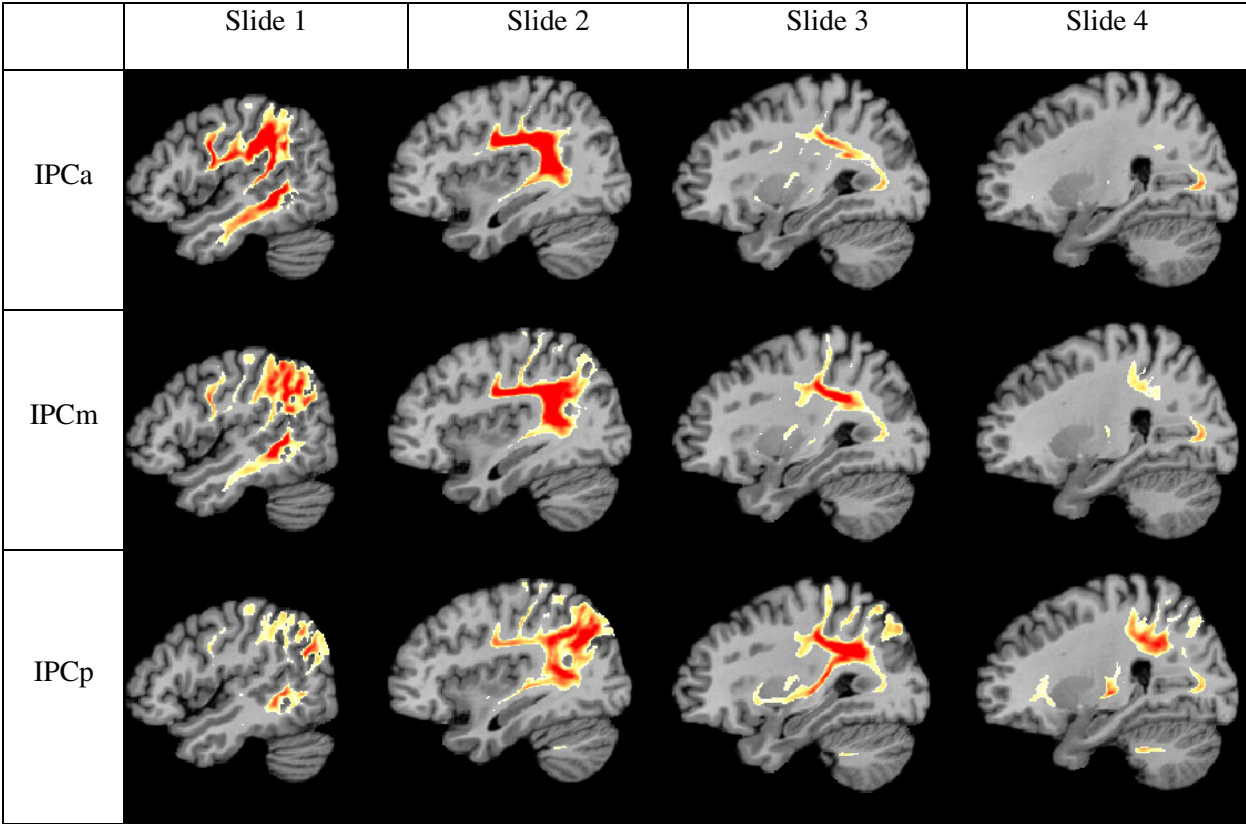


Figure S2: A para-sagittal slice view of the connections of the three different IPCC areas showing the connections of IPCa and IPCm with the superior longitudinal fasciculus (SLF).

## Supplementary Material (2)

To manuscript: “Connectivity architecture and subdivision of the human inferior parietal cortex revealed by diffusion MRI“

The full 3D population maps in MNI space of all IPCC areas are publicly available at:

[http://openscience.cbs.mpg.de/ipcc/IPCC\\_Parcellation\\_Population\\_Maps.zip](http://openscience.cbs.mpg.de/ipcc/IPCC_Parcellation_Population_Maps.zip)